Journal of Applied Sciences

ISSN 1812-5654

science alert

ANSInet
an open access publisher
http://ansinet.com

Journal of Applied Sciences 8 (12): 2202-2216, 2008
ISSN 1812-5654

Petrology, Geochemistry and Mineral Chemistry of Extrusive Alkalic Rocks of the Southern Caspian Sea Ophiolite, Northern Alborz, Iran: Evidence of Alkaline Magmatism in Southern Eurasia

Mojgan Salavati
Department of Geology, Isfahan University, Azadi Square, Isfahan, Iran

Abstract: The alkalic basalts of the SCO ophiolite are made up of olivine, clinopyroxene (salite), plagioclase and Fe-Ti oxides. They show a narrow range of SiO_2 (45.2-48.85 wt. %) and MgO (3.59-4.85 wt. %) and are relatively enriched in TiO_2 (3.13-3.82 wt. %). The rocks are enriched in incompatible trace elements such as Zr, Nb and Y. There is no evidence of significant crustal contamination; this may be related to the rapid ascent of the parental magma. Normalized trace element patterns and diagnostic elemental ratio are very similar to those of modern Ocean-Island Basalts (OIB) a feature which suggests that the mantle source region was the asthenosphere. Comparison with the different types of OIB indicates that the basalts may be derived from a high U/Pb (HIMU) source with slightly elevated K and Ba contents. The overall chemical characteristics suggest that the alkali basalts of the SCO were derived from a fertile mantle source and suggest that the magma was produced by a small-degree partial melting of a garnet lherzolite source. As inferred from geochemical and tectonic data, alkali rocks of the SCO were generated from a plume in a local extension regime.

Key words: Neotethyse, partial melting, plume, ophiolite, Guilan

INTRODUCTION

It is now well established that ophiolites represent preserved sections of oceanic crust that have been tectonically emplaced into thrust mountain belts during ocean closure, plate collision and orogenesis. Iranian ophiolites are part of the Tethyan ophiolites of the Middle East (Shojaat *et al*., 2003), that have been tectonically emplaced into the thrust mountain belts of Iran. Tethyan evolution in Iran and neighboring Turkey, Oman and Baluchistan is very complex and hard to work out (Khalatbari-Jafari *et al*., 2004). The main tectonic elements of Iran and the locations of the major Iranian ophiolites are shown in Fig. 1.

The ophiolite complexes are generally dominated by tholeiitic basalts of either mid-ocean ridge or, more commonly suprasubduction zone affinities. The results of most of the petrological and geochemical studies on the Iranian ophiolites show Mid-Ocean Ridge Basalt (MORB) and Island Arc Tholeiite (IAT) affinities (Rahgoshay *et al*., 2007; Shahabpour, 2005; Ghazi *et al*., 2004; Shojaat *et al*., 2003; Ghazi *et al*., 2003; Hassanipak and Ghazi, 2000). Recently suprasubduction ophiolites were reported from the Khoy ophiolite (Khalatbari-Jafari *et al*., 2003, 2004, 2006) and the Anarak, Jandaq and Posht-e-Badam complexes (Bagheri and Stampfli, 2007).

In a number of the better studied examples of phiolite complexes there is recognition that the tholeiitic rocks are tectonically associated with alkalic volcanic rocks which exhibit within-plate characteristics (Aldanmaz *et al*., 2008). In Iran both alkali and tholeiitic rocks were recognized from some ophiolites. Both MORB- and within plate-type basalts in the lavas from the Baft ophiolite were recognized (Ghasemi and Talbot, 2005). Ghazi and Hassanipak (1999) recognized two distinct types of basalts (alkaline and subalkaline extrusives) in the Kermanshah ophiolite.

In this study an ophiolite was studied which is a new ophiolite complex that was reported by Salavati (2000) and was called The Southern Caspian Sea Ophiolite (SCO). This ophiolite is located in the Alborz Range in Northern Iran and was generated in the Upper Cretaceous and can be compared with other Iranian Mesozoic ophiolites (Salavati, 2000).

The Alborz range of the Northern Iran is a region of actively deformed region within the broad Arabia-Eurasia collision zone (Allen *et al*., 2003; Zanchi *et al*., 2006). The Alborz range is an active orogenic belt that contains a number of ophiolites, which during the continental collision between Arabia and Eurasia occurred along the Alborz Suture Zone, have been tectonically emplaced into Alborz mountain belts.

The SCO ophiolite is exposed to an area that is located in the Southern Amlash city, in Guilan province,

North of Iran. The geology of the area is still poorly known, because of its location in rain forest and dense topography.

Both tholeiitic and alkalic suites have been reported from the Southern Caspian Sea ophiolite (Salavati, 2000; Salavati *et al.*, 2008). Although the greater part of this ophiolite is volcanic, minor plutonic rocks occur in both suites.

The petrology and geochemistry of the SCO alkali basalts have not been investigated in any detail and the tectonic setting of the magmatism is yet to be determined. The purpose of this contribution is to present a detailed mineralogical and chemical study of the SCO alkali basalts, to assess the tectonic setting of magma generation.

MATERIALS AND METHODS

Field mapping and systematic rock sampling in the SCO were conducted during two field seasons in 2006 and 2007. Almost 150 samples of the SCO alkali extrusive rocks have been collected. After petrographic studies, some samples were selected and prepared for chemical analyses.

Seven samples from alkali extrusive rocks were selected for major and trace element analyses. Two samples were performed by inductively coupled plasma atomic emission spectrometry (ICP-AES, analyst: J. Cotten) at the Université Bretagne Occidentale, Brest, France. Rock powders were dissolved into solution in closed flasks by acid attack (HF and HNO_3) and redissolution by an aqueous solution of boric acid. The detection limits are discussed in Cotten *et al.* (1995). In addition, Rb contents were determined by AAS. Five samples were analysed in ALS Chemex in Canada by lithium fusion and a combination of ICP-MS (Table 3).

Mineral phases were analyzed for major and minor elements on polished thin sections by electron microprobe at the Microsonde e´lectronique de l'ouest (Centre Ifremer de Brest, France), with a Camebax SX-50.

RESULTS

Geological setting: The Southern Caspian Sea ophiolite complex is a dismembered ophiolite complex and is located in the north part of the Iranian Guilan Province. The SCO occurs as the lense body that has NNW-SSE trend and is one of the best-preserved oceanic crustal remnants of the Mesozoic Iranian ophiolites (Fig. 1).

The study of different parts of the SCO ophiolite was difficult because of poor accessibility and dense rain forest. The full suite of ophiolite lithologies is present only on the shores of the Caspian in the East Guilan (Salavati and Soofi, 2007).

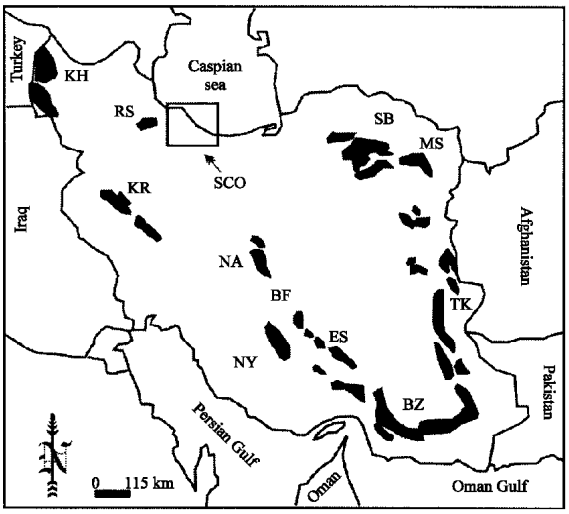

Fig. 1: Distribution of the ophiolite belts in Iran after Emami *et al.* (1993) and location of the SCO area. Main Iranian ophiolite complexes: BZ: Band-e-Ziyarat (also called Kahnuj complex). KR: Kermanshah, NA: Nain, NY: Neyriz, SB: Sabzevar, TK: Tchehel Kureh, RS: Rasht, MS: Mshhad, KH: Khoy, BF: Baft, ES: Esfandegheh, (SCO: Southern Caspian Sea Ophiolite)

The study of schematic stratigraphic columns of the SCO show that, the SCO is almost a complete oceanic lithospheric section including, from bottom to top (east to west): layered ultramafic cumulates, layered gabbros, isotropic gabbros, sheeted dike complex and extrusive rocks (Fig. 3) covered by Campanian-Maestrichtian limestone bearing fossils of Globotruncana (Salavati, 2000; Salavati and Soofi, 2003; Kananian *et al.*, 2005).

Volcanic rocks are the most widespread rock-type in the SCO ophiolite (Fig. 2). The alkali volcanic rocks occur as pillow lava and massive lava and the pillow forms are dominant and are more abundant than the other forms. Pillows show complete zonation from surface to core generally with a clear chilled margin. In the bottom of extrusive unite a transitional zone between diabase dikes and pillow lavas are observed that gradually convert to pillow lava units. The SCO dike complex shows primary contact a relationship with the isotropic gabbro at it's top. Furthermore, alkali gabbro is found in this area (Salavati, 2000).

Petrography: Almost 150 samples of the SCO alkali extrusive rocks have been collected. After petrographic studies, some samples were selected and prepared for chemical analysis.

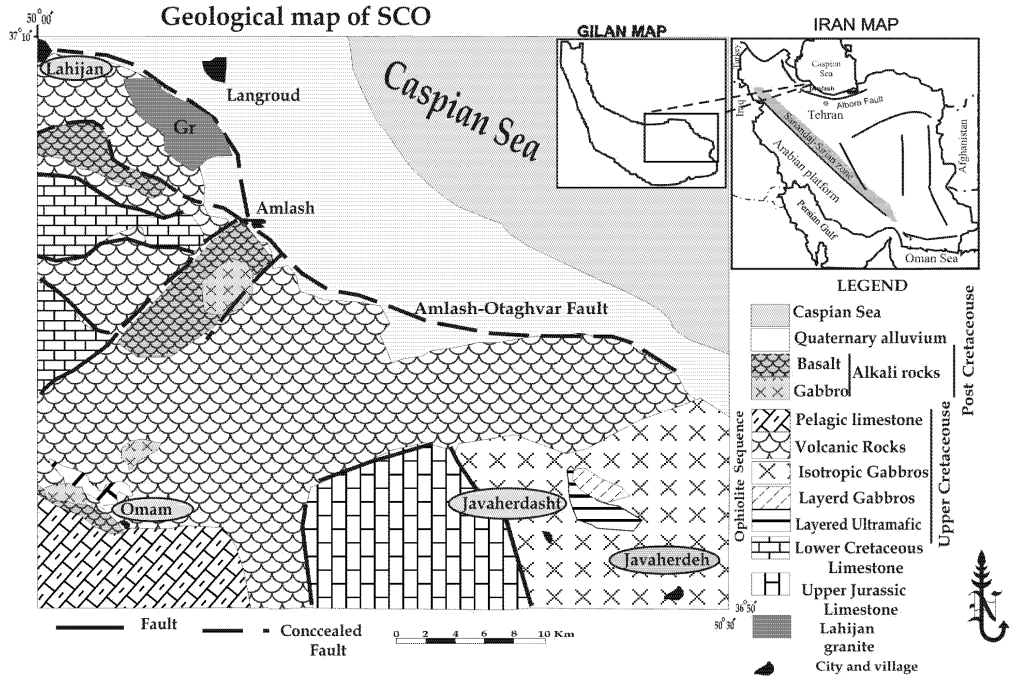

Fig. 2: The geological map of Southern Caspian Sea ophiolite complex, showing the main geological unite of SCO

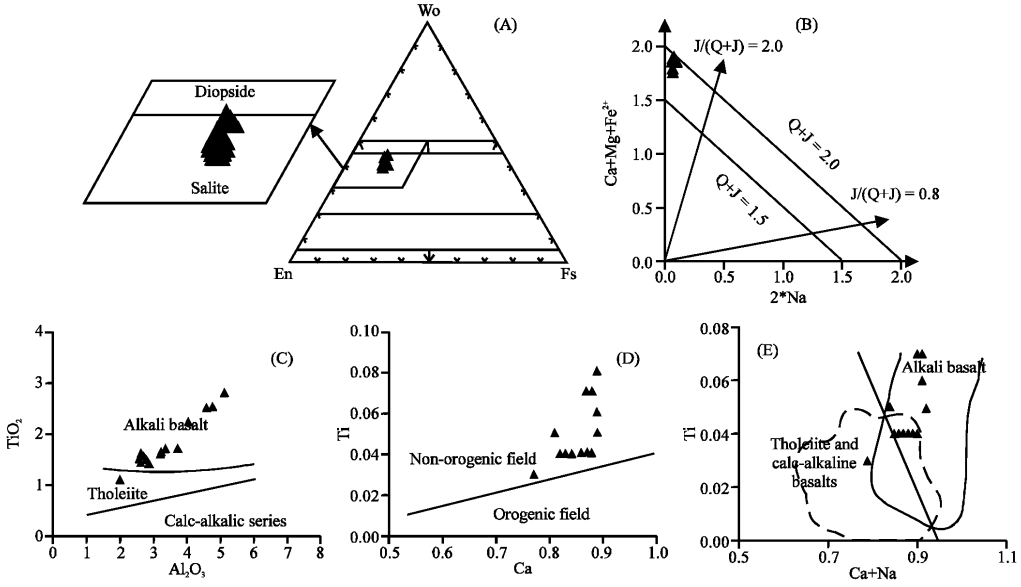

Fig. 3: (A), (B) Composition of the clinopyroxenes from Southern Caspian Sea ophiolite are depicted on the En-Wo-Fs clinopyroxene classification diagram after Morimoto (1988). (C): TiO_2 v. $A1_2O_3$ binary diagram after Le Bas (1962); (D): Ti v. total Al and (E) Ti v. Ca+Na binary diagrams from Leterrier *et al*. (1982)

Petrographically, the alkali basalts are predominantly phyric, with phenocrysts forming 18 to 40 vol. % of the rock. The major phenocryst phases are plagioclase and clinopyroxene with some rocks also containing olivine microphenocrysts. The phenocryst phases are embedded in a microcrystalline to cryptocrystalline groundmass,

consisting primarily of plagioclase laths, small grains of clinopyroxene, olivine and opaque iron oxides, in addition to minor amounts of alteration products. The basaltic rocks exhibit a variety of textures including porphyritic, glomeroporphyritic, ophitic, subophitic, intersertal, pilotaxitic and rarely aphyric. Clinopyroxene (24-30 vol. % of the rock) is also abundant both as a phenocryst and as a groundmass phase. The clinopyroxenes are similar to titanaugite and have a clear high Ti rim. The olivine microphenocrysts (5-25 vol. % of the rock) are altered to iddingsite. Plagioclase makes up about 15 to 45 vol. % of the rock, occurring mostly as groundmass material (0.1 to 0.4 mm long microlaths) and rarely as microphenocrysts or phenocrysts (0.6 to 1 mm long). The Fe-Ti oxides are the abundant phase in groundmass.

Mineral chemistry

Clinopyroxene: The end-member composition for clinopyroxenes from the alkali basaltic rocks is $Wo_{38.1-43.98}$ $En_{42.21-47.09}Fs_{12.57-15.54}$ (Table 1). The clinopyroxenes on the Q = Ca+Mg+Fe^{2+} v. J = 2Na diagram plot in Ca-Mg-Fe pyroxene field (Fig. 3b) and are mainly plotted in the salite field on the En-WO-Fs diagram (Morimoto, 1988; Fig. 3A); its Mg-number (Mg/(Mg+Fe^{2+})) ranges from 0.72 to 0.77 and CaO content from 19.6 to 22.2 wt. % (Table 1). The salite is relatively enriched in Ti (1.07-2.82 wt. % TiO_2) and in Al (1.93-5.1 wt. % Al_2O_3). This is typical of clinopyroxene in alkali basaltic lavas (Abdel Fattah *et al*., 2004). Na_2O contents are generally low (0.25-0.83 wt. %); this low Na_2O content indicates low pressure of crystallization (p<5 Kbar (Kananian *et al*., 2005)). On the Al_2O_3 v. TiO_2 binary diagram (Fig. 3B) of Le Bas (1962), the analysed clinopyroxcnes fall in the alkaline field. Furthermore, on the total Ca+Na v. Ti plot (Fig. 3C); most clinopyroxenes fall in the alkaline basalt field of Letterrier *et al*. (1982). Most clinopyroxenes on the Ca-Ti discrimination diagram (Fig. 3D) fall in the non-orogenic field. The clinopyroxenes show temperature ranges from 603 to 831°C (Kananian *et al*., 2005).

Plagioclase: Plagioclase compositions occupy a range of An_{57-72} (Fig. 4). Plagioclase phenocrysts have a range of compositions (Table 2), from An_{63-72} in core to An_{57-69} in rim. In general, plagioclases have common normally zoning type, calcic core to sodic rim. The plagioclases have a very small Or-component (0.1 K ions per formula unit), but a somewhat high iron content (0.46 to 0.82 wt. % FeO as total iron).

Major-element geochemistry: Table 3 contains major and trace element data for 7 reprehensive samples of the alkali basaltic rocks of the SCO. They have narrow major element compositional ranges, which vary from 45.2 to 48.85 wt. % SiO_2, 13.35-18.45 wt. % Al_2O_3, 3.2-4.85 wt. % MgO, 9.68-14.75 wt. % Fe_2O_3 (as total iron), 8.05-9.7 wt. % CaO and 2.79-3.82 wt. % TiO_2 (Table 3). They are

Table 1: Results of microprobe analysis and number of cations per formula unit of clinopyroxene based on 6 oxygen

Sample No.	1	2	3	4	5	6	7	8	9	10	11	12	13	14	15
SiO_2 (wt%)	50.70	50.50	52.25	51.43	50.57	51.62	51.44	51.12	49.11	47.35	48.58	50.70	48.77	51.83	49.85
TiO_2	1.61	1.41	1.07	1.40	1.71	1.43	1.45	1.50	2.52	2.82	2.53	1.49	2.23	1.60	1.72
Al_2O_3	3.15	2.80	1.93	2.77	3.29	2.57	2.76	2.70	4.55	5.10	4.70	2.52	4.01	2.59	3.69
$FeO_{(t)}$	8.40	8.55	9.86	8.77	8.88	8.57	8.09	7.84	8.62	8.80	8.19	9.00	8.79	8.08	8.45
MnO	0.13	0.31	0.19	0.12	0.24	0.07	0.10	0.20	0.27	0.12	0.06	0.48	0.10	0.15	0.12
MgO	14.70	14.70	15.78	15.02	14.46	14.69	15.01	14.27	13.24	12.83	13.37	13.67	13.46	14.15	13.43
CaO	20.70	20.70	19.63	20.78	20.34	21.32	21.30	21.70	22.07	22.22	21.67	21.80	22.19	21.98	22.22
Na_2O	0.37	0.28	0.25	0.37	0.35	0.37	0.33	0.28	0.45	0.43	0.40	0.31	0.34	0.31	0.83
K_2O	0.00	0.00	0.01	0.00	0.00	0.02	0.00	0.00	0.01	0.00	0.00	0.00	0.00	0.00	0.00
Cr_2O_3	0.20	0.00	0.00	0.12	0.20	0.07	0.19	0.00	0.02	0.00	0.03	0.00	0.06	0.00	0.00
NiO	0.00	0.00	0.26	0.00	0.00	0.15	0.00	0.00	0.00	0.01	0.00	0.00	0.02	0.07	0.06
Total	100.00	99.20	101.20	100.77	100.04	100.86	100.66	100.06	100.84	99.67	99.52	100.05	99.99	100.75	99.92
Si	1.88	1.89	1.92	1.89	1.88	1.90	1.89	1.89	1.82	1.77	1.82	1.89	1.82	1.92	1.86
Ti	0.04	0.04	0.03	0.04	0.05	0.04	0.04	0.04	0.07	0.08	0.07	0.04	0.06	0.04	0.05
Al^{IV}	0.12	0.11	0.08	0.11	0.12	0.10	0.11	0.11	0.18	0.23	0.18	0.11	0.18	0.08	0.14
Al^{VI}	0.02	0.01	0.00	0.01	0.03	0.01	0.01	0.01	0.02	0.00	0.03	0.00	0.00	0.03	0.02
Fe^{3+}	0.03	0.04	0.04	0.04	0.02	0.03	0.03	0.03	0.06	0.10	0.04	0.04	0.08	0.01	0.05
Fe^{2+}	0.23	0.23	0.26	0.23	0.26	0.23	0.22	0.21	0.21	0.18	0.21	0.24	0.19	0.26	0.21
Mn	0.00	0.01	0.01	0.00	0.01	0.00	0.00	0.01	0.01	0.00	0.00	0.02	0.00	0.00	0.00
Mg	0.81	0.82	0.86	0.82	0.80	0.81	0.82	0.81	0.73	0.72	0.75	0.76	0.75	0.78	0.75
Ca	0.83	0.83	0.77	0.82	0.81	0.84	0.84	0.86	0.88	0.89	0.87	0.88	0.89	0.87	0.89
Na	0.03	0.02	0.02	0.03	0.03	0.03	0.02	0.02	0.03	0.03	0.03	0.02	0.02	0.02	0.03
K	0.00	0.00	0.00	0.00	0.00	0.00	0.00	0.00	0.00	0.00	0.00	0.00	0.00	0.00	0.00
Cr	0.01	0.00	0.00	0.00	0.01	0.00	0.01	0.00	0.00	0.00	0.00	0.00	0.00	0.00	0.00
Ni	0.00	0.00	0.01	0.00	0.00	0.00	0.00	0.00	0.00	0.00	0.00	0.00	0.00	0.00	0.00
Mg#	75.70	75.20	74.14	75.23	74.07	75.70	76.64	77.14	73.00	72.00	75.00	73.08	73.53	75.73	74.26
Wo	43.68	43.23	39.90	42.93	42.86	43.98	43.98	42.41	38.83	38.10	40.11	39.58	39.27	41.05	39.47
En	42.63	42.71	44.56	42.93	42.33	42.21	42.93	45.03	46.81	47.09	46.52	45.83	46.60	45.79	46.84
Fs	13.69	14.06	15.54	14.14	14.81	13.61	13.09	12.57	14.36	14.81	13.37	14.58	14.14	13.16	13.68

Table 2: Representative results of microprobe analysis and number of cations per formula unit of plagioclase based on 8 oxygen

Sample No.	SM1	SM2	SM3	SM4	SM5	SM6	SM7	SM8	SM9	SM10	SM11	SM12	SM13	SM14	SM15
SiO_2 (wt. %)	52.64	52.44	50.15	52.89	52.40	52.45	53.36	51.95	50.97	53.37	53.01	53.49	50.82	53.17	54.60
Al_2O_3	28.08	27.88	28.94	28.57	28.78	29.18	27.53	28.93	28.92	29.28	29.35	28.37	30.45	28.71	28.78
FeO	0.71	0.70	0.52	0.82	0.80	0.67	0.71	0.46	0.47	0.69	0.79	0.68	0.77	0.48	0.72
CaO	13.13	13.21	13.98	12.47	12.70	13.17	12.83	13.64	14.66	12.98	13.37	12.60	14.86	12.68	12.22
Na_2O	3.80	3.79	3.31	4.10	3.98	3.77	4.08	3.57	3.34	3.91	3.72	4.22	2.99	4.15	4.66
K_2O	0.32	0.31	0.34	0.32	0.32	0.32	0.35	0.32	0.30	0.35	0.37	0.36	0.26	0.45	0.39
BaO	0.00	0.00	0.00	0.00	0.00	0.00	0.00	0.00	0.00	0.00	0.00	0.00	0.00	0.00	0.00
Total	98.68	98.33	97.24	99.17	98.98	99.56	98.86	98.87	98.66	100.58	100.61	99.72	100.15	99.64	101.37
Si	9.71	9.71	9.42	9.69	9.63	9.59	9.81	9.57	9.45	9.64	9.59	9.75	9.28	9.70	9.78
Al	6.10	6.08	6.40	6.17	6.23	6.28	5.97	6.28	6.31	6.23	6.26	6.09	6.55	6.17	6.07
Fe(ii)	0.10	0.10	0.08	0.12	0.12	0.10	0.10	0.07	0.07	0.10	0.11	0.10	0.11	0.07	0.10
Ca	2.59	2.62	2.81	2.44	2.50	2.57	2.52	2.69	2.91	2.51	2.59	2.46	2.90	2.47	2.34
Na	1.35	1.36	1.20	1.45	1.41	1.33	1.45	1.27	1.20	1.37	1.30	1.49	1.05	1.46	1.61
K	0.07	0.07	0.08	0.07	0.07	0.07	0.08	0.07	0.07	0.08	0.08	0.08	0.06	0.10	0.08
Ba	0.00	0.00	0.00	0.00	0.00	0.00	0.00	0.00	0.00	0.00	0.00	0.00	0.00	0.00	0.00
An	64.40	64.63	68.61	61.51	62.61	64.64	62.19	66.59	69.60	63.40	65.08	60.97	72.20	61.18	57.86
Ab	33.72	33.55	29.39	36.60	35.50	33.48	35.78	31.54	28.69	34.56	32.77	36.95	26.29	36.23	39.93
Or	1.86	1.80	1.98	1.87	1.87	1.87	2.02	1.86	1.69	2.03	2.14	2.07	1.50	2.58	2.19

Table 3: Representative major oxide and trace element data from the Southern Caspian Sea alkali basalts

Sample No.	SM21	SM22	SM23	S'M24	SM25	SM26	SM27
SiO_2 (wt%)	48.10	48.85	46.50	46.50	48.70	45.90	45.20
TiO_2	3.37	3.37	3.44	3.13	3.16	3.75	3.82
Al_2O_3	15.15	15.10	13.65	13.35	14.70	15.50	14.80
Fe_2O_3	12.98	12.36	14.75	13.70	12.20	13.30	12.90
MnO	0.18	0.18	0.25	0.22	0.13	0.16	0.18
MgO	3.84	3.59	4.73	4.85	3.41	4.27	4.21
CaO	8.92	8.05	9.70	9.58	8.64	8.28	8.50
Na_2O	2.98	3.04	2.68	2.57	2.92	3.88	4.03
K_2O	1.48	1.73	1.22	1.22	1.60	1.32	1.49
Cr_2O_3	0.00	0.00	0.00	0.01	0.01	0.099	0.01
P_2O_5	0.56	0.59	0.59	0.56	0.56	0.57	0.61
LOI	2.06	2.64	2.26	2.24	2.05	3.23	3.98
Total	99.62	99.50	99.77	98.00	98.20	100.25	99.90
Ba (ppm)	485.00	460.00	348.00	333.00	456.00	448.00	471.00
Ce	68.00	69.00	64.80	62.10	65.90	58.90	60.50
Co	33.00	37.00	42.00	42.70	35.10	39.50	36.00
Cr	50.00	27.00	30.00	40.00	50.00	30.00	40.00
Dy	5.85	6.05	6.29	6.90	6.30	5.30	5.15
Er	2.80	2.90	3.05	3.19	2.93	2.43	2.31
Eu	2.75	2.80	2.79	2.95	2.91	2.57	2.48
Gd	7.65	7.90	7.77	8.56	8.35	6.45	7.17
La	33.50	36.00	30.50	30.10	31.60	27.80	30.70
Nb	46.00	47.00	42.30	41.40	45.30	43.50	43.60
Nd	38.50	40.00	34.60	34.10	36.80	30.90	31.10
Ni	21.00	24.00	48.00	46.00	22.00	40.00	29.00
Rb	18.00	32.00	22.40	23.90	26.70	23.50	26.70
Sm	8.30	8.50	7.82	8.17	8.21	6.97	6.93
Sr	700.00	690.00	553.00	536.00	662.00	882.00	917.00
Th	3.60	3.75	2.84	2.90	3.76	2.70	2.99
V	240.00	250.00	266.00	251.00	224.00	270.00	251.00
Y	28.00	30.00	28.20	27.60	25.80	23.00	22.90
Yb	2.21	2.30	2.16	2.39	2.25	1.66	1.70
Zr	200.00	200.00	183.00	187.00	194.00	176.00	180.00
Zn	_	_	154.00	160.00	150.00	131.00	148.00
W	_	_	1.00	5.00	2.00	7.00	3.00
U	_	_	0.71	0.71	0.92	0.66	0.65
Tl	_	_	0.40	<0.50	<0.50	0.40	<0.50
Tm	_	_	0.35	0.39	0.37	0.30	0.28
Ta	_	_	2.50	2.60	2.70	2.60	2.50
Tb	_	_	1.18	1.21	1.13	0.97	0.99
Sn	_	_	2.00	2.00	2.00	2.00	2.00
Pb	_	_	4.99	<5.00	5.00	4.00	<5.00
Pr	_	_	7.96	8.00	8.46	7.55	7.36
Lu	_	_	0.30	0.33	0.31	0.24	0.24
Mo	_	_	2.00	2.00	2.00	2.00	<2.00
Hf			5.60	5.30	5.40	4.50	4.90

Table 3: Continued

Sample No.	SM21	SM22	SM23	S'M24	SM25	SM26	SM27
Ho	_	_	1.10	1.20	1.09	0.86	0.90
Ga	_	_	25.70	23.40	22.90	21.90	21.70
Cs	_	_	0.13	0.15	0.09	0.48	0.65
Cu	_	_	109.00	105.00	44.00	71.00	66.00
Mg#	22.82	22.50	24.28	26.14	21.84	24.30	24.60

Fe_2O_3 is total iron; Mg# = (Mg/Mg+Fe^{2+}))*100

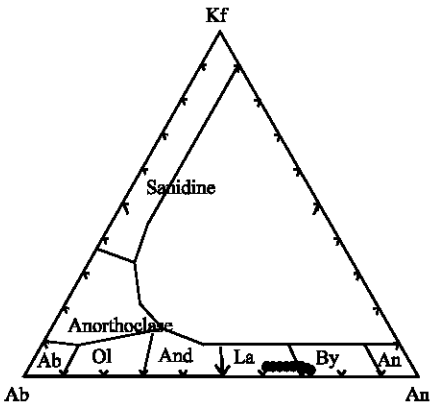

Fig. 4: Feldspar compositions from the SCO alkali basalts

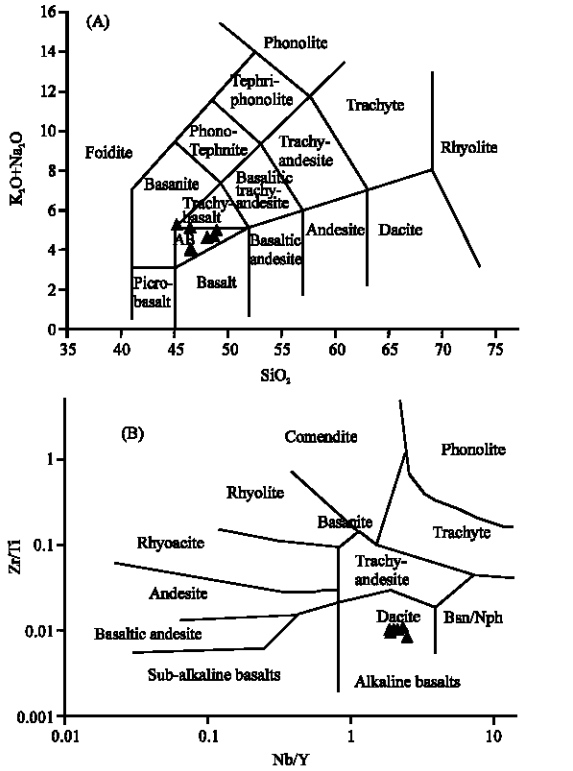

Fig. 5: (A) Geochemical classification of SCO basalts using (B) TAS diagram (Le Bas *et al*., 1986) and (B) Zr/Ti V. Nb/Y diagram (Winchester and Floyd, 1977)

characterized by high Na_2O+K_2O contents. In the classification diagram of Le Bas and Streckeisen (1991), the basalt samples are restricted in composition and mostly fall in alkali basalt field and overlap with the field of basalt (Fig. 5a). The alkaline nature of the investigated rocks is also indicated in the (Nb/Y)-(Zr/Ti) diagram (Winchester and Floyed, 1977; Fig. 5b). The SCO alkali basalts have moderately low MgO (3.2-4.85 wt. %) and the Mg numbers (=molar Mg/(Mg+Fe^{2+}), are generally low, ranging from 0.32 to 0.49 (with an average of 0.23). Such values indicate that the rocks do not represent primary magmas, but may have experienced some degree of olivine and clinopyroxene fractionation.

Trace-element geochemistry: Although an attempt has been made to minimize the effect of alteration by screening the samples for primary volcanic features, such as pillow structures and for absence of secondary mineralization, relatively high loss-on-ignition values (2.05-3.98 wt. %) for most of the basaltic rocks imply a possible sea-floor alteration. Previous works indicate that the transition metals (V, Cr, Mn, Fe, Co, Ni, Zn), Mg, Y and the High Field Strength (HFS) elements (Zr, Nb, Ti, Hf, P and REE) are relatively immobile and largely reflect magmatic abundances. By contrast, Large Ion Lithophile (LIL) elements (Ba, Rb, K and Sr) have generally experienced metasomatic and hydrothermal mobilization in most of the samples (Saccani and Photiades, 2004; Parlak *et al*., 2004; Farahat *et al*., 2004; Krienitz *et al*., 2006; Dawoud *et al*., 2006; Manikyamba *et al*., 2004; Kadarusman *et al*., 2004; Yibas *et al*., 2003). Thus, we consider it unlikely that the measured mobile element abundances are pristine and we based our modelling and interpretation largely on immobile HFSE, REE and Th.

The alkali basalts of the SCO exhibit a relatively narrow trace element compositional range: Cr = 27-50 ppm, V = 224-270 ppm, Sr = 536-917 ppm, Ba = 333-485 ppm and Rb = 18-32 ppm. The alkali basalts of the SCO are generally enriched in the High Field Strength Elements (HFSE) such as Zr (176-200 ppm), Y (23-30 ppm) and Nb (41.4-47 ppm; Table 3). The investigated alkali basalts have elemental ratios, such as La/Nb and Zr/Nb (averages of 0.71 and 4.3, respectively), similar to the average of HIMU-OIB (La/Nb = 0.72 and Zr/Nb = 4.1; Moghazi,

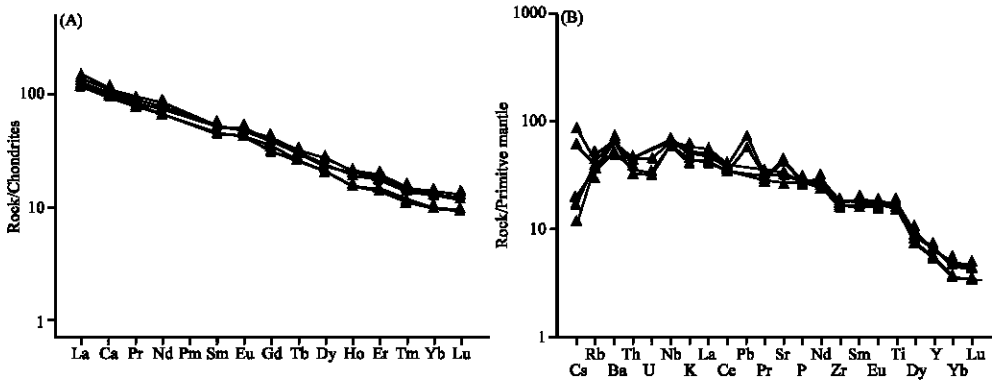

Fig. 6: (A) Chondrite-normalized REE patterns for basalts, (B) Incompatible element patterns of basalts normalized to primitive mantle; Normalizing values of chonderite and primitive are from Sun and McDonough (1989)

2003a), (HIMU refer to high $^{238}U/^{204}Pb$ mantle and member and has the lowest $^{87}Sr/^{86}Sr$ of OIB; Abdel Fattah *et al*., 2004).

Conderite-normalized REE patterns for alkali basalts of the SCO are illustrated in Fig. 6A. Total REE contents of the alkali volcanic rocks have range from 9 to 110 times chondrite. They have an LREE enriched pattern with (La_N/Yb_N)=5.5-7.9. REE profiles are linear and homogeneous with a moderate positive slope from HREE to LREE and overall, the REE patterns are subparallel (Fig. 6). In general, enrichment in the LREE is a characteristic feature of OIB- type alkali basalts (Sun and McDonough, 1989; Abdel Fattah *et al*., 2004). The primitive mantle-normalized incompatible element patterns of the rocks (Fig. 6B) indicate that the investigated rocks are generally enriched in the incompatible element compared to primitive mantle abundances with peaks at Nb, Pb, Nd, Ti, Ba and Sr, with relative depletion in LILE (Rb, Th, U, Zr). In contrast, despite there being no petrographic evidence for plagioclase accumulation, most of the sample are characterized by positive Sr anomalies. Thus, the relatively high Sr content in these basalts is a feature inherited from the mantle source.

Characterization of the magma source region: The REE data (Table 3) of the investigated alkali basaltic rocks show the source region of the rocks should be located in the garnet-lherzolite zone (Moghazi, 2003a). The most diagnostic feature of residual garnet is the fractionation of Heavy Rare-Earth Elements (HREE) because of their strong partitioning into garnet (Abdel Fattah *et al*., 2004). The presence of garnet as a residual phase in the melt source region is inferred from the $(Tb/Yb)_N$ ratio (Abdel Fattah *et al*., 2004; Moghazi, 2003a). The investigated rocks have $(Tb/Yb)_N$ ratio ranging between 2.12 to 2.47, which is comparable to those of the alkali basalts of Hawaii ($(Tb/Yb)_N$=1.89-2.45; Abdel Fattah *et al*., 2004; Moghazi, 2003a) and which are considered to have been generated in a garnet-bearing lherzolitic mantle source (Moghazi, 2003a). This means a depth of at least 80 km (Moghazi, 2003a), indicating that magma generation should have occurred well within the asthenosphere.

In order to explore the source characteristics of the investigated alkali basalts based on their geochemical characteristics, critical trace element ratios are compared with those of well-known OIB occurrences. Based on Sr, Nd and Pb isotopes, the asthenospheric sources of OIB may be divided into four reservoirs, two reflect enrichment mantle type of OIB, EMI and EMII that may represent the addition of small amounts of subducted sediments: pelagic in the case of EMI and terrigenous in the case of EMII, one refers to a subduction component with high $^{238}U/^{204}Pb$ (HIMU) and one is a depleted MORB mantle (DMORB) (Abdel Fattah *et al*., 2004; Moghazi, 2003a). These types may also be identified using element ratios (Moghazi, 2003a). Ce/U, Th/Nb, Rb/Sr, Zr, Nb and Y compositions are among the most useful ratio that can be effective in distinguishing between mantle and crustal magma sources (Moghazi, 2003a; Abdel Fattah *et al*., 2004). The Zr, Nb and Y compositions of the investigated alkali basaltic rocks resemble HIMU-OIB, as they exhibit relatively higher concentrations of Y than transitional- or normal-MORB (T-MORB or N-MORB; Menzies and Kyle, 1990). The investigated basalts have elemental ratios (Zr/Nb = 4.27, La/Nb = 0.71 and Rb/Nb = 0.56, on average) similar to those characteristic of HIMU-OIB (Moghazi, 2003a).

Some high field strength (HFS) elements, such as Nb, are found to be highly variable in lithospheric mantle melts. Therefore, the variations in the La/Nb ratio have been interpreted by some authors to reflect the style of metasomatic enrichment (Abdel Fattah *et al*., 2004). HFS

elements (such as Nb) are depleted in the lithospheric mantle relative to the light REE (La) high Nb/La ratio (approximately>1) indicate an OIB-like asthenospheric mantle source for basaltic magmas and the lower ratio (approximately<0.5) indicate a lithospheric mantle source (Abdel Fattah *et al*., 2004). The Nb/La and La/Yb ratio in basalts of the SCO (averages of 1.4 and 15.19, respectively) are consistent with an astenospheric mantle (OIB-like) source (Fig. 7D); the investigated basalts also plot within the field of HIMU-OIB that can be observed in Fig. 7b. Furthermore, the alkali basalts of the SCO have a Ce/U ratio lower than N-MORB and mostly plot within the OIB field (Fig. 7a). They also fall within the range of OIB field in Rb/Sr v. SiO_2 diagram (Fitton *et al*., 1991; Fig. 7C). Comparison of the element ratio with values for different types of OIB (Table 4) shows that the alkali basalts of the SCO may be derived from a HIMU-OIB source with high Ba content.

Table 4: Incompatible element ratios of the SCO alkali basalts compared to different types of OIB

	SCO alkali basalts		HIMU OIB	EMI OIB	EMII OIB	PM	N-MORB
	Range	Mean	Mean	Mean	Mean	Mean	Mean
Zr/Nb	4.05-4.51	4.27	4.10	6.90	6.10	14.80	30.00
La/Nb	0.63-0.76	0.71	0.72	0.94	0.98	0.94	1.07
Ba/Nb	8.04-10.5	9.68	5.60	13.20	9.70	9.00	4.30
Ba/Th	121.27-165.92	134.21	64.00	128.00	74.00	770.00	60.00
Rb/Nb	0.39-0.68	0.56	0.37	1.01	0.73	0.91	0.36
K/Nb	239.00-293	269.00	139.00	301.00	293.00	323.00	296.00
Th/Nb	0.06-0.08	0.072	0.09	0.112	0.134	0.117	0.071
Th/La	0.09-0.11	0.10	0.12	0.115	0.137	0.125	0.067
Ba/La	11.06-15.34	13.65	7.80	14.10	8.20	9.60	4.00

Values of OIB (HIMU, EMI, EMII), primodial mantle (PM) and mid-ocean ridge basalt (N-MORB) are from Weaver (1991)

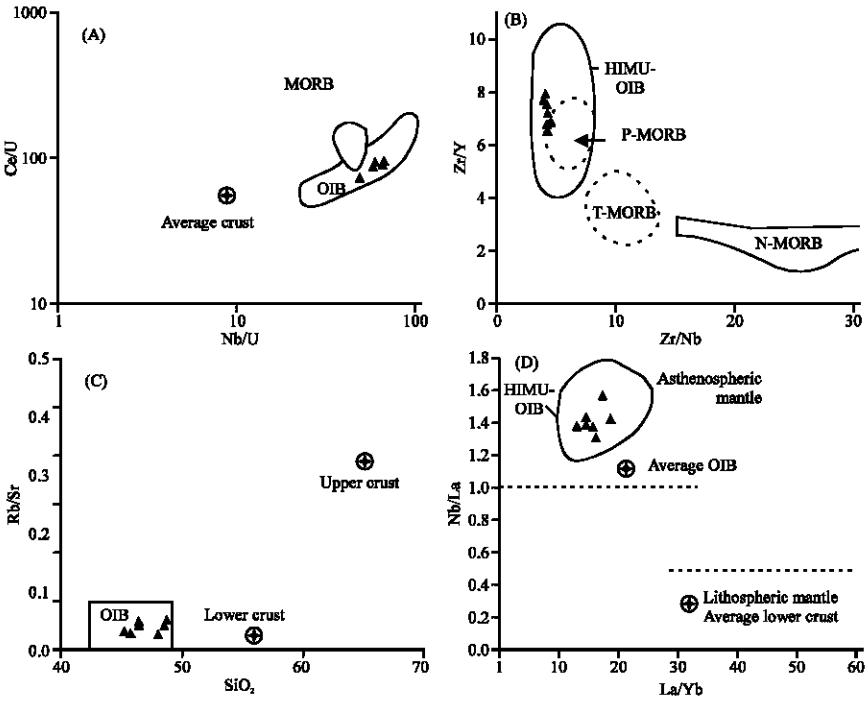

Fig. 7: Binary diagrams of (A) Nb/U v. Ce/U for the SCO basalts, compared with MORB, average crust (Hofmann *et al*., 1986) and OIB (Hofmann *et al*., 1986), (B) Zr/Y v. Zr/Nb diagram showing that the studied samples plot mostly near the T-MORB field. The field of OIB is from Abdel-Rahman and Nadaer (2002) and the other fields are transitional MORB (T-MORB) and normal MORB (N-MORB) and are taken from Menzies and Kyle (1990), (C) SiO_2 v. Rb/Sr for the investigated alkali basalts compared with OIB (Fitton *et al*., 1991) and upper and lower crust (Taylor and McLennan, 1985), (D) Nb/La v. La/Yb variation diagram. The composition of the SCO alkaline basalts. Average OIB is after Fitton *et al*. (1991) and average lower crust representing average of six lower crustal granulite xenoliths) is after Chen and Arculus (1995)

Thus, trace element data of the alkali basalts of the SCO suggest that these rocks have chemical characteristics similar to HIMU-OIB and providing an addition argument for their derivation from the asthenospheric mantle source. They are distinctly from the lower and upper crust.

Role of crustal contamination: Magma differentiation is related to three main processes: fractional crystallisation, magma mixing and contamination (Gourgaud and Vincent, 2004). Alteration and crustal contamination are secondary processes, which may have contributed to the chemical composition of the SCO alkali basalts suite.

Certain chemical parameters can be used to assess the degree of contamination. For example, basaltic rocks affected by crustal contamination, exhibit K/P ratio>7, La/Ta>22 and La/Nb> 1.5 (Abel-Fattah *et al*., 2004). The low values of such elemental ratio in the basaltic rocks of the SCO (K/P = 3.8-5.3; La/Ta = 10.62-12.28; La/Nb = 0.63-0.76) suggest that the role of crustal contamination during magma evolution has been minimal.

In addition, incompatible trace elements such as Th, Ta and Yb will be considered to determine crustal contamination. Crustal contamination affects Th more than Ta and Yb so which the samples have crustal contamination show high Th/Yb values (Moghazi, 2003a). Ytterbium is used as a normalizing factor to minimize the effects of fractional crystallization and crystal accumulation (Pearce, 2005; Aldanmaz *et al*., 2008). In the diagram that shows the variation of Th/Yb v. Ta/Yb (Pearce, 1983), the investigated basalts plot inside the mantle array field (Fig. 8) suggesting minimal crustal contamination. The OIB-type alkaline rocks are characterized by strong enrichments in highly incompatible elements relative to less incompatible elements (higher LREE/HREE ratios than that of MORB). They plot on the MORB-OIB mantle trend on a Th/Ybv. Ta/Yb diagram, indicating that their mantle source had no subduction influence and the resulting magmas were not affected by any significant contamination of lithospheric material. Higher ratios of both Ta/Yb and Th/Yb relative to MORB compositions, however, may be explained by a number of processes including magma generation by: (1) small degrees of melting of a convectively homogenized source that is enriched in incompatible elements relative to depleted MORB source; or (2) small degrees of partial melting of a mantle source that leaves garnet-bearing residue (Aldanmaz *et al*., 2000); or (3) systematic mixing between increments of melt derived from a compositionally uniform source by variable degrees of melting (Aldanmaz *et al*., 2005, 2006).

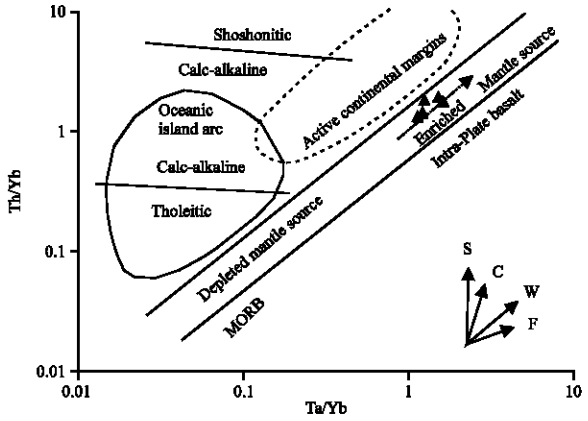

Fig. 8: Ta/Yb v. Th/Yb diagram after Pearce (1983); vectors show trends produced by subductionzone enrichment (S), crustal contamination (C), within-plate enrichment (w) and fractional crystallization (F)

Despite the lack of isotopic data, some trace elements enable the possible role of crustal contamination in SCO magma petrogenesis to be evaluated. High Th/Yb ratios would be indicative of crustal contamination (Gourgaud and Vincent, 2004).

All geochemical characteristics imply that crustal contamination did not play a major role in the magma evolution of the SCO alkali basalts.

Negligible crustal contamination shows that magma ascent may have been rapid enough from the site of partial melting to the surface to escape contamination.

Petrogenetic considerations: role of partial melting: Alkali basaltic rocks are known to be extremely diverse geochemically and derive from diverse mantle sources (Frey *et al*., 2000; Abdel Fattah *et al*., 2004). The nature of the mantle source material, whether it is dominanted by recycled oceanic or continental crust, or by recycled sedimentary components and the processes associated with melting and migration of melt, determine the composition of the basaltic lavas. Abdel Fattah *et al*. (2004) displayed that a number of geochemical parameters have been used in order to assess the role of petrogenetic processes such as fractional crystallization and partial melting the evolution of mafic lavas. During the partial melting processes, the highly/moderately incompatible element ratios (such as Ba/Zr, Ba/Zr and P_2O_5) are known decrease with the increasing degree of partial melting (Abdel Fattah *et al*., 2004). It has been that partial melting is still by far the most efficient process for fractionating highly/moderately incompatible element ratios (Abdel Fattah *et al*., 2004). Figure 9A, C shows a linear positive

trend between the Ba/Y and Ba/Zr ratio and Ba, the observed relative fractionation in such a ratio is a function of partial melting degree. The ratio of an incompatible element during melting to Al_2O_3 (which is usually buffered by residual garnet) typically decreases systematically with increasing degree of partial melting (Abdel Fattah *et al*., 2004). The linear positive trends between Zr/Al_2O_3 and Nb/Al_2O_3 v. P_2O_5/Al_2O_3 (Fig. 9B, D) is indicative of the significant role of partial melting processes (Abdel Fattah *et al*., 2004) in the production of magma chemistry observed in the SCO alkali basalts.

Relative fractionation of HFSE is a common feature in both continental and oceanic basalts (Hawaii: Scotland, Atlantic OIB, North Sea, Antarctica; Moghazi, 2003a). Such is considered to be a function of the amount of residual garnet and clinopyroxene in the mantle source as a result of different degree of partial melting (Moghazi, 2003a). Since Y is retained in garnet (K_D = 1.083), the negative correlation of partial melting such as Ce/Y and Nb/Y ratios (Moghazi, 2003a) v. Zr/Nb in the investigated rocks (Fig. 10 A, B) suggest that partial melting may explain the variation in the alkali basaltic rocks of the SCO. Samples with the highest Ce/Y and Nb/Y and lowest Zr/Nb show a smaller degree of partial melt.

Thus the observed data from the alkali basalts of the SCO show that the source of these rocks was fertile, garnet-bearing asthenospheric mantle.

Tectonic setting: Various investigators have used immobile trace elements (Zr, Y, Ti, REE etc.) to deduce

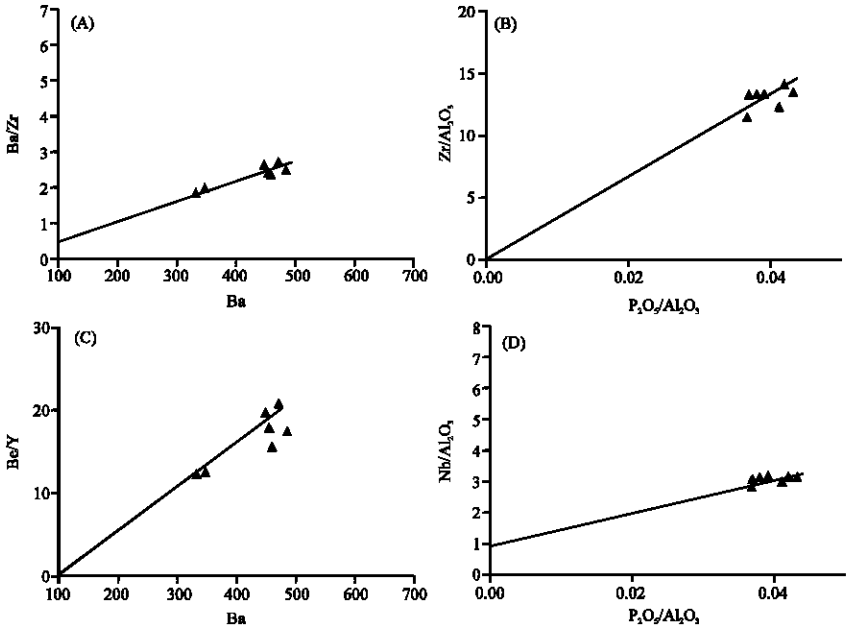

Fig. 9: (A,C) plots showing high/moderately incompatible element ratios v. highly incompatible element concentration for the SCO alkali basalts. Zr/Al_2O_3 and Nb/Al_2O_3 v. P_2O_5/Al_2O_3 diagrams (B, D) for the investigated basalts

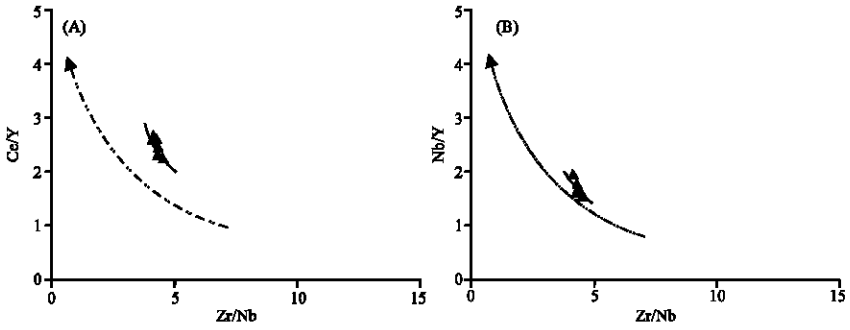

Fig. 10: Binary diagrams of Zr/Nb v. (A) Ce/Y and (B) Nb/Y for alkali samples. The vectors labeled CPX represent fractional removal of clinopyroxene

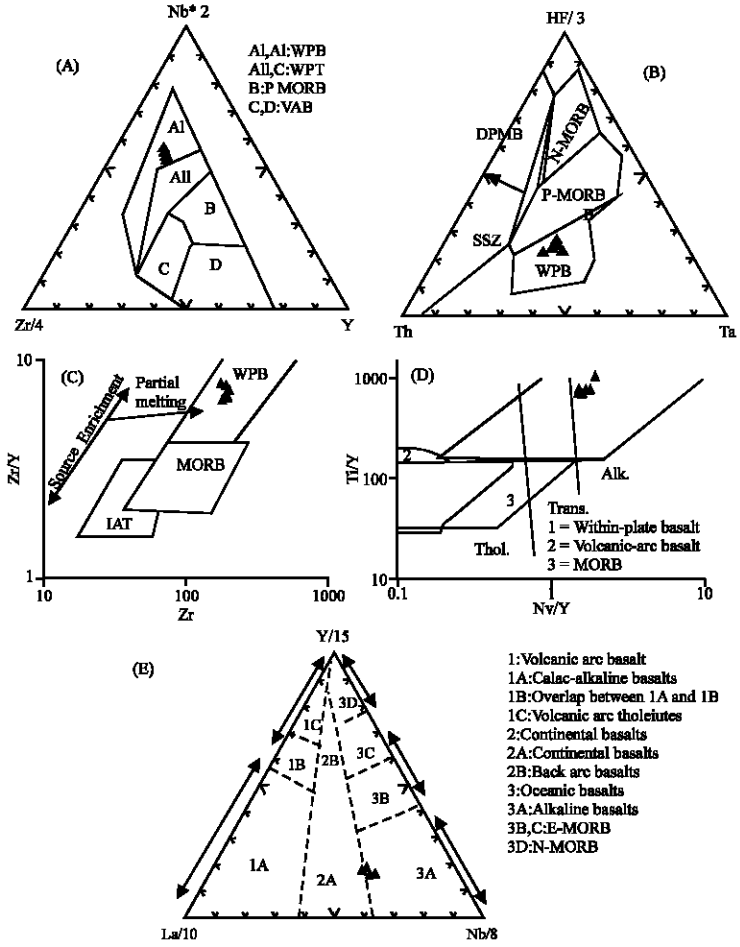

Fig. 11: Geochemical discrimination diagram of basalt of SCO in, (A) Nb-Zr-Y diagram (Meshede, 1986), (B) Th-Hf/3-Ta diagram developed by Wood (1980), (C) Zr/Y versus Zr diagram (Pearce and Norry, 1979), (D) Ti/Y verses Nb/Y diagram (Pearce, 1982) and (E) Ternary plot of La-Y-Nb (after Cabanis and Lecolle, 1989) used to discriminate further between volcanic arc basalts, oceanic basalts and continental basalts

tectonic environments for volcanics and have developed a variety of discriminate diagrams (Pearce and Cann, 1973; Pearce and Norry, 1979; Pearce, 1982; Moghazi, 2003b; Manav *et al*., 2004).

In a Zr-Nb-Y discrimination diagram (Meschede, 1986), the investigated basaltic rocks plot in within-plate basalts (Fig. 11A). In Th-Hf/3-Ta diagram developed by Wood (1980), all of the samples also fall into the within plate field (Fig.11B). In the Zr/Y-Zr (Pearce and Norry, 1979) (Fig. 11C), samples plot in the within plate basalts and shows a within plate nature and shows an enriched mantle source for the alkalic rocks. In Ti/Y versus Nb/Y diagram (Pearce, 1982) (Fig. 11D) samples fall in within-plate basalts in alkali field. In the ternary plot of Y/15-La/10-Nd/8 (11E; after Cabanis and Lecolle, 1989), the investigated rocks fall in the alkaline basalt field in oceanic environment.

DISCUSSION

Alkalic rocks make up a minor component of some ophiolites (Cyprus, Oman and Newfoundland) and are also known from present-day oceanic crust (Hawaii, Iceland and volcanic chains in the South Pacific; Thompson *et al*., 1997). Their relationship with dominant tholeiitic rocks varies. In the SCO ophiolite there are significant quantities of alkalic rocks, both volcanic and plutonic, which form an integral part of the ophiolite. The age relationship between the tholeiitic and alkalic basalts is equivocal, with some massifs having field relationships consistently indicating that the alkalic rocks are younger than the tholeiites (Salavati, 2000). The calc-alkaline rocks of the SCO ophiolite have subtle but distinct negative Nb anomalies indicating a supra-subduction environment of formation (Salavati, 2000). The association of alkalic rocks

lacking the subduction signature with these tholeiites suggests a variety of potential sources in a back arc environment. Thus, from the evidence of the normalized incompatible trace element diagram and the discrimination plots, it appears that the alkalic rocks of the SCO have WPB signatures. Furthermore o the investigated alkali rocks display OIB (HIMU-OIB) affinities.

In some, ophiolite was proposed the presence of deep mantle plumes to account for the enriched chemical nature of the rocks observed at the surface, such mantle plumes are unlikely to exist in a subduction setting (Thompson *et al*., 1997). Some theories (Thompson *et al*., 1997) on the mechanisms of subduction suggest that slab sink rather than pushes through the mantle and migrates oceanward through the rollback effect. The effect is to create a flow of undepleted mantle material into the expanded supra-subduction wedge (Fig. 11). A small amount of melting of this mantle produces alkalic magmas. The REE patterns of the alkalic rocks suggest that melt generation occurs within the garnet stability field. If these magmas erupt close to or at the spreading centre, tholeiitic and alkalic rocks will spatially overlap (The North Philippine Sea and The Northland ophiolite; Thompson *et al*., 1997). Alkalic rocks erupting off axis will be slightly younger than the tholeiilic rocks (e.g. the Salahi lavas in the Oman ophiolite and the crust of the Japan Sea). Based on this theory we thus suggest that the alkali rocks of the SCO were generated from a plume in a local extension regime.

CONCLUSIONS

The Southern Caspian Sea ophiolite of Northern Iran consists mainly of tholeiitic basalts with subordinate alkalic volcanic rocks. The alkalic rocks occur together with, but are generally younger than the tholeiites.

The alkali basalts of the SCO are mostly phyric and consist of about 5-20 vol. % olivine, 24-30% clinopyroxene (salite), 15-45 % plagioclase (labradorite) and 5% opaque Fe-Ti oxide phases.

Geochemically, the investigated rocks have a narrow range of major element compositions (SiO_2, 45.2-48.85 wt. %; MgO, 3.59-4.85 wt. %) and are alkaline in nature. These rocks are enriched in Ti (3.13-3.82 wt. % TiO_2), Zr (176-200 ppm), Nb (41.4-47 ppm) and Y (23-30 ppm). These features reflect strong affinities to OIB. The primitive mantle-normalized pattern are fractionated ($(La/Yb)_N$ = 10.15-14.55).

Elemental ratios (such as K/P, La/Nb, Nb/Y and Th/Nb) suggest that crustal contamination did not play a significant role during magma evolution. There is no evidence of significant crustal contamination or interaction with the subcontinental lithosphere.

All chemical composition of the alkali basalts of the SCO is similar to those of HIMU-OIB.

The overall chemical characteristics suggest that the alkali basalt of the SCO were derived from a fertile mantle source and suggest that the magma was produced by a small-degree partial melting of a garnet lherzolite source. Variation in the basalt compositions arise from different degrees of partial melting.

The alkali basalts of the SCO show the geochemical characteristics of within-plate lavas. As inferred from geochemical and tectonic data, alkali volcanism is interpreted to have been associated with a localized tensional regime.

ACKNOWLEDGMENT

The authors wish to thank the Office of Graduate Studies of the Isfahan University for their support.

REFERENCES

Abdel-Fattah, M., A.M. Abdel-Rahman and P.E. Nassar, 2004. Cenozoic Volcanism in the Middle East: Petrogenesis of alkali basalts from Northern Lebanon. Geol. Mag., 141: 545-563.

Abdel-Rahman, A.M. and F.H. Nader, 2002. Characterization of the Lebanese Jurassic-Cretaceous carbonate stratigraphic sequence: A geochemical approach. J. Geol., 37: 69-91.

Aldanmaz, E., J.A. Pearce, M.F. Thirlwall and J.G. Mitchell, 2000. Petrogenetic evolution of late Cenozoic, post-collision volcanism in Western Anatolia, Turkey. J. Volcanol. Geotherm. Res., 102: 67-95.

Aldanmaz, E., 2002. Mantle source characteristics of alkali basalts and basanites in an extensional intracontinental plate setting, Western Anatolia, Turkey: Implications for multi-stage melting. Int. Geol. Rev., 44: 440-457.

Aldanmaz, E., A. Gourgaud and N. Kaymakci, 2005. Constraints on the composition and thermal structure of the upper mantle beneath NW Turkey: Evidence from mantle xenoliths and alkali primary melts. J. Geodyn., 39: 277-316.

Aldanmaz, E., N. Köprüba i, O.F. Gürer, N. Kaymakci and A. Gourgaud, 2006. Geochemical constraints on the Cenozoic, OIB-type alkaline volcanic rocks of NW Turkey: Implications for mantle sources and melting processes. Lithos, 86: 50-76.

Aldanmaz, E., M.K. Yaliniz, A. Güctekin and M.C. GÖncüo lu, 2008. Geochemical characteristics of mafic lavas from the Neotethyan ophiolites in western Turkey: Implications for heterogeneous source contribution during variable stages of ocean crust generation. Geol. Mag., 145: 37-54.

Allen, M.B., M.R. Ghassemi, M. Shahrabi and M. Qorashi, 2003. Accommodation of late Cenozoic oblique shortening in the Alborz range, Northern Iran. J. Struct. Geol., 25: 659-672.

Bagheri, S. and G.M. Stampfli, 2007. The Anarak, Jandaq and Posht-e-Badam metamorphic complexes in central Iran: New geological data, relationships and tectonic implications. Tectonophysics, 10.1016/j.tecto.2007.11.047.

Cabanis, B. and M. Lecolle, 1989. Le diagramme La/10-Y/15-Nb/8: un outil pour la discrimination des séries volcanique et la mise en évidence des processus de me´lange et/ou de contamination crustale. C.R. Acad. Sci. Ser. II, 309: 2023-2029.

Chen, W. and R.J. Arculus, 1995. Geochemical and isotropic characteristics of lower crustal xenoliths, San Francisco Volcanic Field, Arizona, USA. Lithos, 36: 203-225.

Cotton, J., A. LeDez. M. Bau, R.C. Maury, P. Dulski, S. Fourcade, M. Bohn and R. Brousse, 1995. Origin of anomalous rare-earth and yttrium enrichment in subaerially exposed basalt: Evidence from French polynesia. Chem. Geol., 119: 115-138.

Dawoud, M., H.A. Eliwa, G. Traversa, M.S. Attia and T. Itaya, 2006. Geochemistry, mineral chemistry and petrogenesis of a Neoproterozoic dyke swarm in the North Eastern Desert, Egypt. Geol. Mag., 143: 115-135.

Emami, M.H., M.M. Sadeghi, and S.J. Omrani, 1993. Magmatic map of Iran, Scale 1/1,000,000. Geological Survey of Iran.

Farahat, E.S., M.M. El Mahalawi, G. Hoinkes and A.Y. Abdel Aal, 2004. Continental back-arc basin origin of some ophiolites from the Eastern Desert of Egypt. Mineral. Petrol., 82: 81-104.

Fitton, J.G., D. James and W.P. Leeman, 1991. Basic magmatism associated with Late Cenozoic extension in the Western United States: Compositional variations in space and time. J. Geophys. Res., 96: 13693-13712.

Frey, F.A., D. Clague, J.J. Mahoney and J.M. Sinton, 2000. Volcanism at the edge of the Hawaiian plume: Petrogenesis of submarine alkalic lavas from the North Arch Volcanic Field. J. Petrol., 41: 667-691.

Ghasemi, A. and C.J. Talbot, 2005. A new tectonic scenario for the Sanandaj-Sirjan Zone (Iran). J. Asian Earth Sci., 26: 683-693.

Ghazi, A.M. and A.A. Hassanipak, 1999. Geochemistry and petrology of subalkaline and alkaline extrusives of Kermanshah ophiolite, Zagros Suture Zone, SW Iran. J. Asian Earth Sci., 17: 319-332.

Ghazi, A.M., E.A. Pessagno, A.A. Hassanipak, S.M. Kariminia, R.A. Duncan and H.A. Babaie, 2003. Biostratigraphic zonation and $^{40}Ar/^{39}Ar$ ages for the Neotethyan Khoy ophiolite of NW Iran. Palaeogeogr. Palaeocl Imatol. Palaeoecol., 193: 311-323.

Ghazi, A.M., A.A. Hassanipak, J.J. Mahoney and R.A. Duncan, 2004. Geochemical characteristics, 40Ar-39Ar ages and original tectonic setting of the Band-e-Zeyarat/Dar Anar ophiolite, Makran accretionary prism, S.E. Iran. Tectonophysics, 393: 175-196.

Gourgaud, A. and P.M. Vincent, 2004. Petrology of two continental alkaline intraplate series at Emi Koussi volcano, Tibesti, Chad. J. Volcanol. Geotherm. Res., 129: 261-290.

Hassanipak, A.A. and A.M. Ghazi, 2000. Petrology, geochemistry and tectonic setting of the Khoy ophiolite, northwest Iran: Implications for Tethyan tectonics. J. Asian Earth Sci., 18: 109-121.

Hofmann, A.W., K.P. Jochum, M. Seufert and W.M. White, 1986. Nb and Pb in ocean basalts: New constraints on mantle evolution. Earth Planet. Sci. Lett., 79: 33-45.

Kadarusman, A., S. Miyashita, S. Maruyama, C.D. Parkinson and A. Ishikawa, 2004. Petrology, geochemistry and paleogeographic reconstruction of the East Sulawesi Ophiolite, Indonesia. Tectonophysics, 392: 55-83.

Kananian, A., M. Salavati, D. Esmaeily and A. Asiabanha, 2005. Mineral chemistry of clinopyroxenes in the igneous rocks of Amlash area, North Iran. J. Sci. Uni. Tehran, 30: 229-246.

Khalatbari-Jafari, M., T. Juteau, H. Bellon and H. Emami, 2003. Discovery of two ophiolite complexes of different ages in the Khoy area (NW Iran), CR Geosciences, Vol. 335. Académie des Sciences, Paris, pp: 917-929.

Khalatbari-jafari, M., T. Juteau, H. Bellon, H. Whitcherch, J. Cotton and H. Emami, 2004. New geological, geochronological and geochemical investigations on the Khoy ophiolites and related formations, NW Iran. J. Asian Earth Sci., 23: 507-535.

Khalatbari-jafari, M., T. Juteau and J. Cotten, 2006. Petrological and geochemical study of the Late Cretaceous ophiolite of Khoy (NW Iran) and related geological formations. J. Asian Earth Sci., 27: 465-502.

Krienitz, M.S., K. Haase, K. Mezger, V. Eckardt and M.A. Shaihk-Mashail, 2006. Magma genesis and crustal contamination of continental intraplate lavas in Northwestern Syria. Contrib. Mineral. Petrol., 151: 698-716.

Le Bas, M.J., 1962. The role of aluminum in igneous clinopyroxenes with relation to their parentage. Am. J. Sci., 260: 267-288.

Le Bas, M.J., R.W. Le Maitre, A. Streckeisen and B. Zanettin, 1986. A chemical classification of volcanic rocks based on the total alkali-silica diagram. J. Petrol., 27: 745-750.

Le Bas, M.J. and A.L. Streckeisen, 1991. The IUGS systematics of igneous rocks. Geol. Soc. London, 148: 825-833.

Leterrier, J., R.C. Mary, P. Thonon, D. Girard and M. Marchal, 1982. Clinopyroxene composition as a method of identification of the magmatic affinities of paleo-volcanic series. Earth Planet. Sci. Lett., 59: 139-154.

Manav, H., B.H. Gültekin and B. Uz, 2004. Geochemical evidence for the tectonic setting of the Harmancik ophiolites, NW Turkey. J. Asian Earth Sci., 24: 1-9.

Manikyamba, C., R. Kerrich, S.M. Naqvi and M. Ram Mohan, 2004. Geochemical systematics of tholeiitic basalts from the 2.7 Ga Ramagiri-Hungund composite greenstone belt, Dharwar craton. Precambrian Res., 134: 21-39.

Menzies, M.A. and R. Kyle, 1990. Continental Volcanism: A Crust-Mantle Probe. In: Continental Mantle, Oxford, Menzies, M.A. (Eds.). Oxford Science Publishers, London, pp: 157-77.

Meshede, M., 1986. A method of discriminating between different types of mid-ocean ridge basalts and continental tholeiites with the Nb, Zr, Y diagram. Chem. Geol., 56: 207-218.

Moghazi, A.M., 2003a. Geochemistry of a Tertiary continental basalt suite, Red Sea costal plain, Egypt: Petrogenesis and characteristics of the mantle source region. Geo. Mag., 140: 11-21.

Moghazi, A.M., 2003b. Geochemistry and petrogenesis of a high-K calc-alkaline Dokhan Volcanic suite, South Safaga area, Egypt: The role of late Neoproterozoic crustal extension. Precambrian Res., 125: 161-178.

Morimoto, N., 1988. Nomenclature of pyroxenes. Mineral. Mag., 52: 535-550.

Parlak, O., V. Höck, H. Kozlu and M. Delaloye, 2004. Oceanic generation in an island arc tectonic setting, SE Anatolian orogenic belt (Turkey). Geol. Mag., 141: 583-603.

Pearce, J.A. and J.R. Cann, 1973. Tectonic setting of basic volcanic rocks determined using trace element analyses. Earth Planet. Sci. Lett., 19: 290-300.

Pearce, J.A. and M.J. Norry, 1979. Petrogenetic implications of Ti, Zr, Y and Nb variations in volcanic rocks. Contribution to Mineral. Petrol., 69: 33-47.

Pearce, J.A., 1982. Trace Element Characteristic of Lava from Destructive Plate Poundaries. In: Andesites, Thorpe, R.S. (Ed.). Wiley, Chichester, UK., pp: 525-548..

Pearce, J.A., 1983. Role of the Sub-continental Lithosphere in Magma Genesis at Active Continental Margins. In: Continental basalts and mantle xenoliths, Hawkesworth, C.J. and M.J. Norry (Eds.). Shiva Publishing, Cheshire, pp: 230-249.

Pearce, J.A., 2005. Mantle preconditioning by melt extraction during flow: Theory and petrogenetic implications. J. Petrol., 46: 973-997.

Rahgoshay, M., H. Shafaii Moghadam and S. Pirasteh, 2007. The distinctive trace elements signature of the less-evolved MORB materials in the south of Birjand ophiolites. Iranian J. Crystall. Mineral., 1: 219-230.

Saccani, E. and A. Photiades, 2004. Mid-ocean ridge and supra-subduction affinities in the Pindos ophiolites (Greece): Implications for magma genesis in a forearc setting. Lithos, 73: 229-253.

Salavati, M., 2000. A survey of geology and petrogenesis of magmatic rocks in southern Amlash. M.Sc. Thesis. University of Tehran, Tehran, Iran, pp: 159.

Salavati, M. and A. Samadi Soofi, 2003. A survey of petrogenesis of volcanic rocks in Southern Lahijan. Lahijan Branch of Islamic Azad University, pp: 110.

Salavati, M. and A.S. Soofi, 2007. A survey of petrogenic and economic of gabrroic bodies in Eastern Gilan province. Lahijan Branch of Islamic Azad University, pp: 121.

Salavati, M., A. Kananian, M. Noghreian, A. Darvishzadeh and A. Samadi Soofi, 2008. Discovery of a Neo-Tethyan ophiolite in the North of Iran and evidence for its formation at a slow-spreading center. General Contributions, Journal of the Virtual Explorer, Electronic Edition, ISSN 1441-8142, Volume 28. http://virtualexplorer.com.au/journal/2008/28/.

Shahabpour, J., 2005. Tectonic evolution of the orogenic belt in the region located between Kerman and Neyriz. J. Asian Earth Sci., 24: 405-417.

Shojaat, B., A.A. Hassanipak, K. Mobasher and A.M. Ghazi, 2003. Petrology, geochemistry and tectonics of the Sabzevar ophiolite, North Central Iran. J. Asian Earth Sci., 21: 1053-1067.

Sun, S.S. and W.F. McDonogh, 1989. Chemical and Isotopic Systematics of Ocean Basalts: Implication for Mantle Composition and Processes. In: Magmatism in Ocean Basins, Saunders, A.D. and M.J. Norry (Eds.). Geol. Soc. London Special Publication, London, pp: 313-345..

Taylor, S.R. and S.M. McLennan, 1985. The Continental Crust: Its Composition and Evolution. Oxford: Blackwell, pp: 312.

Thompson, G.M., J. Malpas and E.M. Smith, 1997. The geochemistry of tholeiitic and alkalic plutonic suites within the Northland ophiolite, Northern New Zealand; magmatism in a back arc basin. Chem. Geol., 142: 213-223.

Winchester, J.A. and P.A. Floyed, 1977. Geochemical discrimination of different magma series and their differentiation products using immobile elements. Chem. Geol., 20: 325-334.

Wood, D.A., 1980. The application of a Th-Hf-Ta diagram to problems of tectonomagmatic classification and to establishing the nature of crustal contamination of basaltic lavas of the British Tertiary volcanic province. Earth Planet. Sci. Lett., 50: 11-30.

Yibas, B., W.U. Reimold, C.R. Anhaeusser and C. Koeberl, 2003. Geochemistry of the mafic rocks of the ophiolitic fold and thrust belts of southern Ethiopia: Constraints on the tectonic regime during the Neoproterozoic (900-700 Ma). Precambrian Res., 121: 157-183.

Zanchi, A., F. Berra, M. Mattei, M.R. Ghassemi and J. Sabouri, 2006. Inversion tectonics in central Alborz, Iran. J. Struct. Geol., 20: 1-15.